Available online at www.sciencedirect.com
SCIENCE DIRECT
Polymer 46 (2005) 7037–7046
polymer
www.elsevier.com/locate/polymer

Effect of matrix features on polypropylene layered silicate nanocomposites

W. Gianelli[a], G. Ferrara[b], G. Camino[a,*], G. Pellegatti[b], J. Rosenthal[c], R.C. Trombini[d]

[a]CDCMP/Politecnico di Torino-sede di Alessandria, Via T. Michel 5, 15100 Alessandria, Italy
[b]Basell R&D, P.le Donegani 12, 44100 Ferrara, Italy
[c]Basell USA Inc., 912 Appleton Rd, Elkton, MD 21921, USA
[d]Departamento de Engenharia de Materiais, Universidade Federal de Sao Carlos, CEP 13565-905 Sao Carlos, Sao Paulo, Brasil

Received 26 November 2004; received in revised form 7 April 2005; accepted 13 May 2005
Available online 27 June 2005

Abstract

The aim of this study was to examine the effect of the polypropylene based resin on the properties of organoclay–PP nanocomposites prepared by melt compounding using a twin screw extruder.

The characterization of the obtained materials was performed by X-ray diffraction (XRD), transmission electron microscopy (TEM), thermogravimetric analysis (TGA), melt flow rate (MFR) and mechanical tests.

The study has shown the effect of the polymer matrix molecular weight on the possibility of producing by melt compounding nanocomposites based on PP homopolymers or heterophasic PP–PE copolymers and an organically modified montmorillonite, in presence of maleic anhydride-modified polypropylene (PP-*g*-MAH).

An increase of mechanical properties was achieved both for homopolymers and heterophasic copolymers. However the reinforcing effect of clay dispersed in heterophasic copolymers was not as high as found for the homopolymers.

Keywords: Melt compounding; Polymer nanocomposites; Polypropylene

1. Introduction

In order to extend the standard polyolefins (PO) properties and to compete with other materials, the most important polyolefin producers are strongly interested in evaluating and exploring nanofillers as an alternative to conventional reinforcing agents like talc, wollastonite, calcium carbonate, etc. This quite recent nanotechnology is appealing as it seems to be able to overcome certain application limits of existing PO grades. Properties enhancement is a consequence of both higher specific surface area and higher aspect ratio, in comparison with conventional fillers [1–3].

Direct dispersion of a phyllosilicate in the molten polymer with an extruder or a discontinuous batch mixer allows to prepare intercalated or exfoliated lamellar nanocomposites [3]. In the first case polymer chains are intercalated in the galleries, in the second case the delaminated silicate is homogeneously dispersed in the matrix [3–7].

The dispersion of clay layers in the molten polymer depends on thermal diffusion of polymer molecules in the interlayer space galleries and on mechanical action due to mixing devices [8]. Thermal diffusion is favoured by making the galleries chemically compatible with the polymer, for example by exchanging interlayers inorganic clay cations with organic cations such as the alkylammonium cations used in commercial 'organoclays' [9,10]. In the case of non polar polymers (e.g. polyolefins) an additional compatibiliser is used to obtain the nanocomposite [11–14].

The mechanical dispersing action depends on processing parameters such as compounding equipment, geometry of mixing elements and rheological characteristics of the polymer [15].

Either intercalated or exfoliated structures were observed

* Corresponding author. Tel.: +39 131 229361; fax: +39 131 229331.
E-mail address: giovanni.camino@polial.polito.it (G. Camino).

0032-3861/$ - see front matter © 2005 Elsevier Ltd. All rights reserved.
doi:10.1016/j.polymer.2005.05.149

when PP, both homopolymers and heterophasic PP–PE copolymers, were compounded with a relatively small amount of organophilic montmorillonite in presence of PP-*g*-MAH which promotes clay exfoliation and adequate interfacial adhesion between filler and polymer [16,17].

The goal of this work is to investigate the effect of polymer structures on nanocomposite properties. In particular, the effect of polymer molecular weight in materials prepared via melt compounding of either homopolymers or heterophasic copolymers in presence of PP-*g*-MAH as a compatibilizer was studied.

2. Experimental

2.1. Materials

Commercially available grades of homo and heterophasic PP produced by Basell Polyolefins S.p.A. were used in this work. The principal features of the virgin polymers are reported in Table 1. All of them are currently manufactured with the same catalytic system and the same technology.

The homopolymers have a different MFR ranging from 0.5 to 25 g/10 min at 230 °C. In the heterophasic copolymers an ethylene propylene rubbery phase is finely dispersed into the homopolymer matrix. The relative amount of rubber (XS, Table 1) is comparable in the three samples (15–17%) whereas MFR is varied from 0.4 to 12 g/10 min at 230 °C.

The selected compatibilizing agent was a PP-*g*-MAH containing 1 wt.-% of grafted maleic anhydride with a MFR of 110 g/10 min at 230 °C (Polybond 3200, Crompton Corp.).

A natural montmorillonite exchanged with dimethyl dihydrogenated tallow quaternary ammonium chloride (Cloisite 20A, Southern Clay Products) was used as nanofiller. It has an average particles diameter of 8 μm and and a cation exchange capacity of 95 mequiv./100 g.

Table 1
Principal properties of neat polymers

Sample	Commercial name	MFR (g/10 min)	XS[a] (%)
Homo 1[b]	Hostalen PP YD50G	0.5	–
Homo 2	Moplen HP501L	6	–
Homo 3	Moplen HP400R	25	–
Hetero 1[c]	Hostalen PP861	0.4	15
Hetero 2	Moplen EP440G	1.5	17
Hetero 3	Moplen EP540N	12	15

[a] XS, relative amount of rubber, wt%.
[b] Homo, homopolymer.
[c] Hetero, heterophasic copolymer PP–PE.

2.2. Melt processing

The composites were prepared in a corotating intermeshing twin screw extruder (Leistritz ZSE18HP-40D, d = 27 mm, l/d = 40) with a screw speed of 400 rpm and a residence time in the range 30–45 s. The processing conditions were optimized for each nanocomposite and they were in any case in the following range of values: molten temperature = 190–218 °C, torque = 23–48%, die pressure = 13–39 bar. The proportions of the composites constituents were chosen as follows: PP = 88 wt.-%, nanofiller = 5 wt.-%, PP-*g*-MAH = 7 wt.-%. The composites were obtained mixing the neat polymers with a premixed master (PP-*g*-MAH and nanofiller), previously prepared in the same extruder. The set thermal profiles of the extruder are reported in Table 2. In order to produce reference materials the neat polymers, PP and PP-*g*-MAH, were undergone the same treatment in the extruder as the composites.

2.3. Characterization

2.3.1. X-ray diffraction (XRD)

XRD analyses were performed at room temperature using a Philips X'Pert X-ray diffractometer, from 2Θ 2° to 2Θ 9°, with a step scan of 0.02°. The X-ray source was a tungsten filament tube with a Cu-target (K_α = 1.542 Å).

2.3.2. Transmission electron microscopy (TEM)

TEM measurements were performed with a high resolution transmission electron microscope Philips TECNAI 100. Ultrathin sections of about 100 nm were cut with a Reichert FCS microtome equipped with a diamond knife.

2.3.3. Mechanical properties

The specimens for the mechanical testing were prepared in accordance with ISO 294 and conditioned for 40 h at 23 ± 2 °C and 50 ± 5% relative humidity following ISO 291.

The flexural and elongational properties were determined

Table 2
Extruder thermal profiles for master and composites

Zone	Setting temperatures (°C)	
	Master	Composites
1	190	195
2	195	195
3	195	195
4	200	200
5	195	200
6	195	200
7	200	210
8	200	210
9	185	220
Die	180	220

in accordance with ISO 178 using an Instron 4301 instrument on injection-moulded specimens, prepared following ISO 294-1 (length = 80 ± 2 mm, width = 10 ± 0.2 mm and thickness = 4.0 ± 0.2 mm).

Impact strength was measured with a Ceast 6545 pendulum-type hammer striking a notched specimen with a 0.05 mm notch (ISO 180). Heat deflection temperature was evaluated with a Ceast HDT 6 placing the specimen in an oil bath under a load of 460 kPa (ISO 75).

Finally, the dimensional stability of the samples was estimated as shrinkage effects during the cooling phase on both the length and the width of the specimens and coefficient of linear thermal expansion (CLTE) in accordance with ASTM D-696.

2.3.4. Thermogravimetric analyses (TGA)

Thermogravimetries were carried out in nitrogen or air (60 cm^3/min) in a Q500 TA Instruments thermobalance, heating from 50 to 800 °C at 10 °C/min.

3. Results and discussion

3.1. Morphology

The resulting morphologies were monitored by means of XRD and TEM for characterizing the nanoscale dispersion of the layered silicate [18]. The X-ray diffraction results of the composites based on homopolymers and the clay used for their preparation are reported in Fig. 1. They show in the case of samples Homo 1 and Homo 2 the formation of a mainly intercalated nanocomposite morphology. In fact the lower 2Θ values diffraction peak of the composite materials indicates a bit larger clay interlayer spacing (d = 2.60 and 2.52 nm respectively) in comparison with Cloisite 20A (d = 2.32 nm).

For the sample at high MFR (Homo 3) the diffraction signal decreases in height as compared to those of the organoclay and of samples Homo 1 and Homo 2 in Fig. 1 and it indicates that extensive delamination should be obtained in this case.

TEM micrographies of samples Homo 1 and Homo 3 are shown in Figs. 2 and 3, respectively. These pictures confirm that delamination of the clay was achieved in both cases with a somewhat better dispersion of the nano-sized particles within the matrix in the case of sample Homo 3.

The X-ray diffraction results of the composites based on heterophasic copolymers and the clay used for their preparation are reported in Fig. 4. For sample Hetero 2 a microcomposite morphology should result because the low 2Θ values diffraction peak indicates the same interlayer spacing of Cloisite 20A (d = 2.32 nm). In the case of heterophasic copolymers only the sample Hetero 1 has a mainly intercalated morphology indeed its diffraction peak value indicates a bit larger interlayer spacing (d = 2.55 nm) in comparison with Cloisite 20A (d = 2.32 nm).

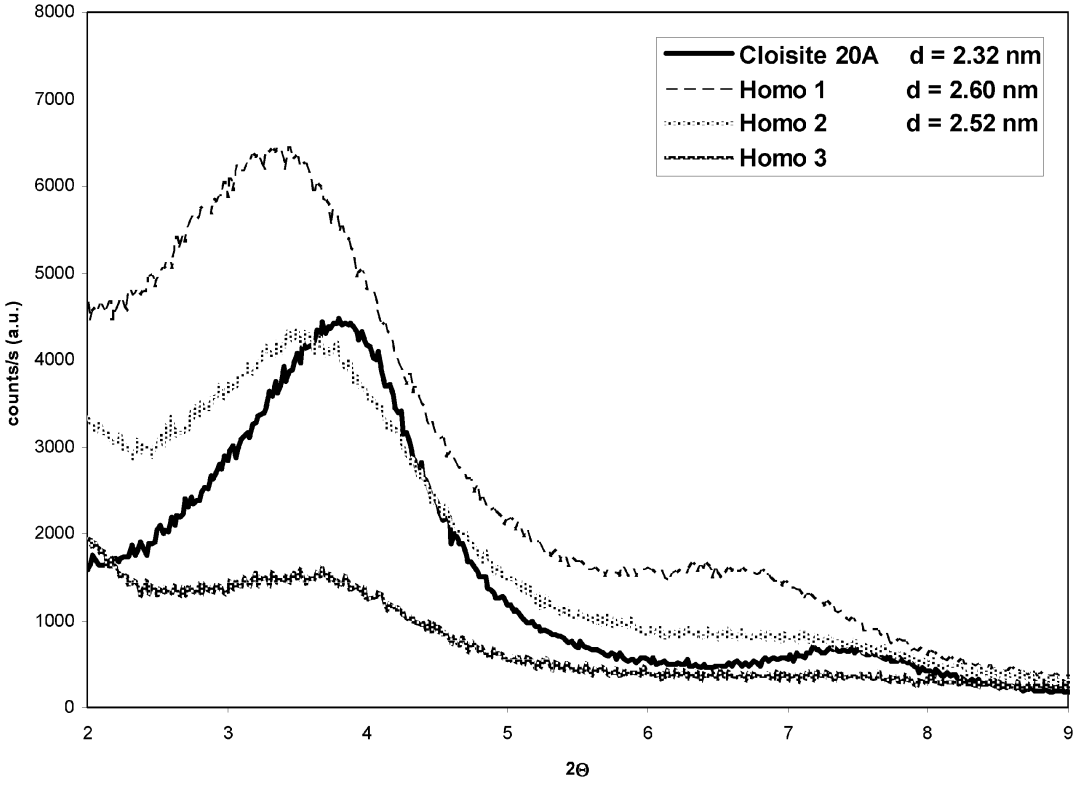

Fig. 1. X-ray diffraction patterns of composites based on homopolymers and the clay used for their preparation (Cloisite 20A).

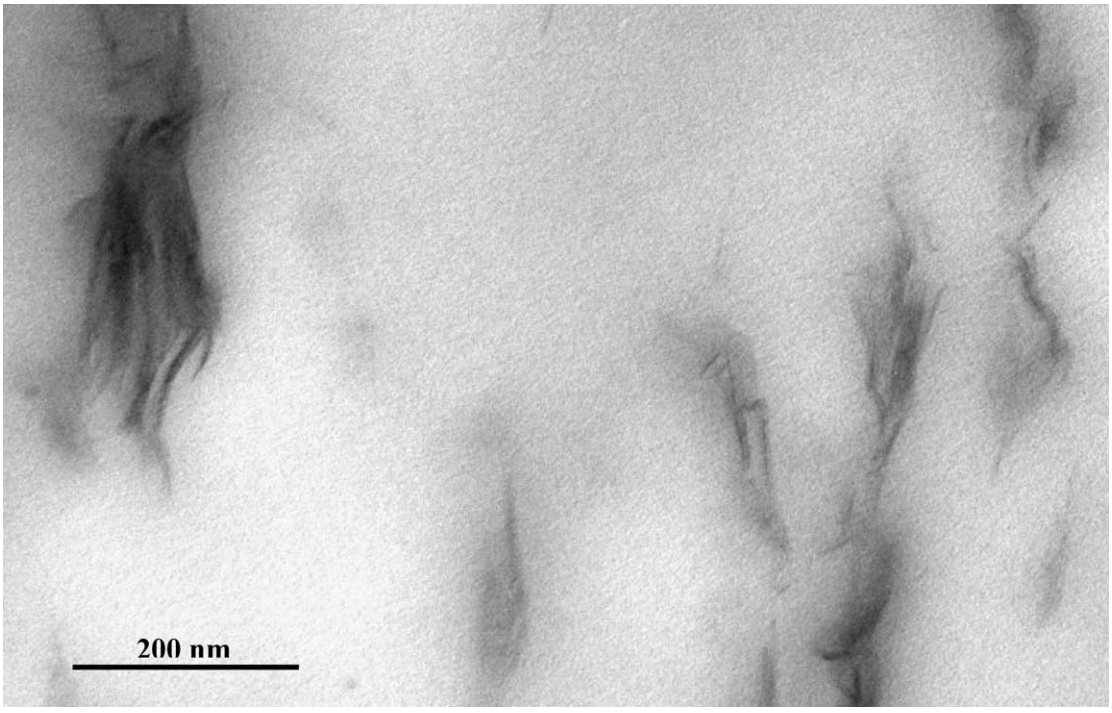

Fig. 2. TEM image for nanocomposite based on sample Homo 1.

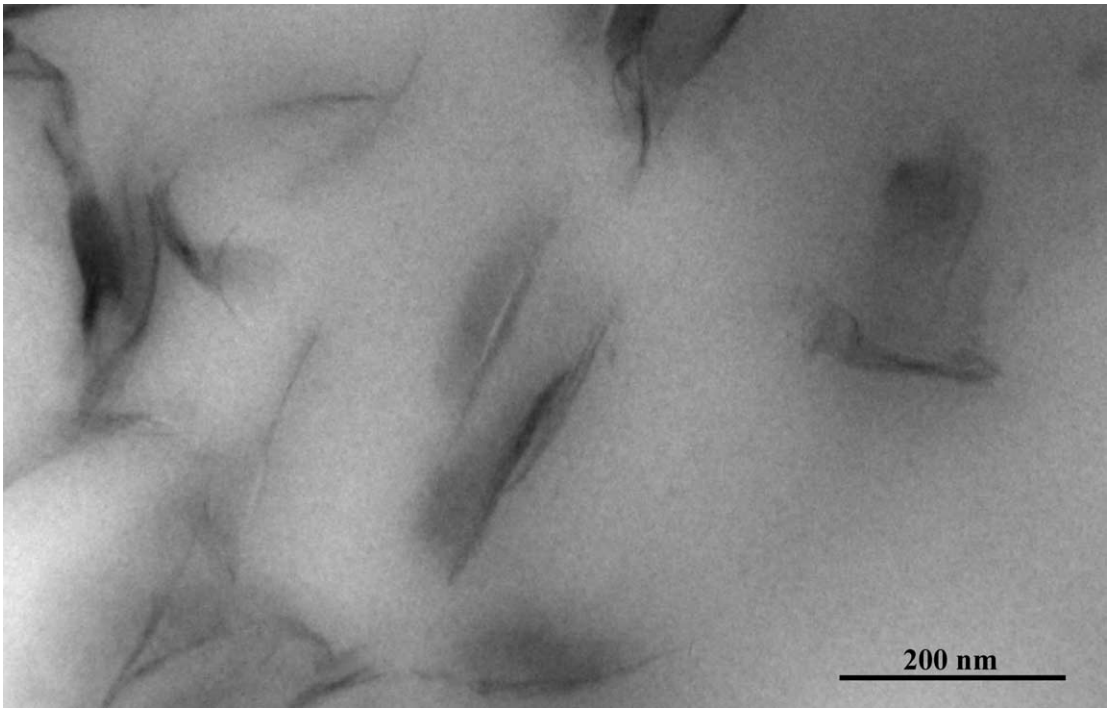

Fig. 3. TEM image for nanocomposite based on sample Homo 3.

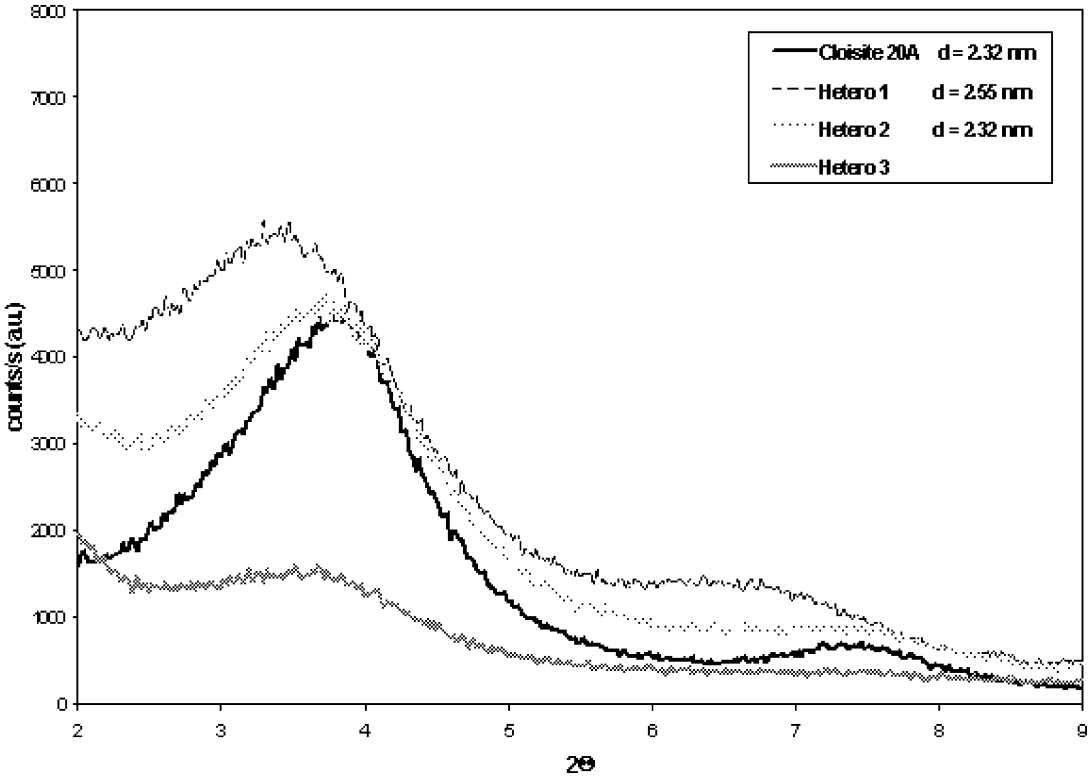

Fig. 4. X-ray diffraction patterns of composites based on heterophasic copolymers and the clay used for their preparation (Cloisite 20A).

Even for heterophasic copolymers extensive delamination seems to be obtained for the sample at high MFR (Hetero 3) as in the case of homopolymers.

3.2. Mechanical properties

In Tables 3 and 4 the results of physical–mechanical testing for both the base polymers (PP homopolymers, or PP–PE, + PP-*g*-MAH) and the composites are reported.

In the top of the tables the responses of the strain–stress behaviour are summarized. The chord modulus represents the ratio of stress to strain at a specified level of strain (3.5%). The impact test results, the heat deflection temperatures, the shrinkage and the coefficient of linear thermal expansion are reported too.

By comparing these results some general considerations can be extracted; for all the composites a remarkable increase of modulus, larger for homopolymers (28–49%) as compared to heteropolymers (24–33%), was observed. The reinforcing effect increases with increasing delamination of the organoclay as shown in Fig. 5 where modulus improvement increases with increasing MFR. Indeed, XRD shows that with increasing MFR, morphology tends to evolve from intercalation to delamination (Figs. 1 and 4).

A trend similar to modulus is shown in Fig. 6 by the increase of yield strength in composites which is related to the quality of the crystals in the crystalline regions [19].

An improvement of the dimensional stability was achieved for composites till to a maximum reduction of 25% for the homopolymer with the highest MFR (CLTE 0–30 °C, Table 3). Furthermore a less evident increase of yield stress and HDT occurred for the composites together with a lower shrinkage.

The decrease of the MFR found in composites can be

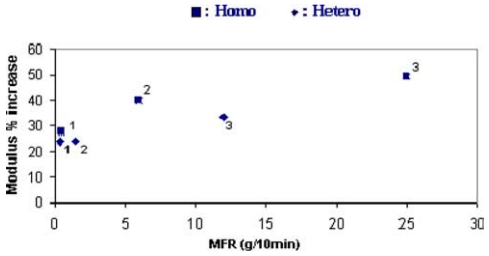

Fig. 5. Modulus enhancement vs. MFR.

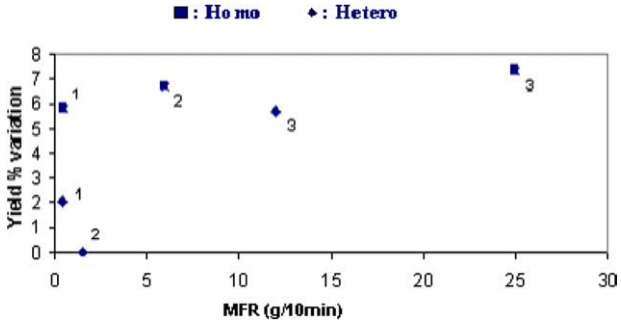

Fig. 6. Yield stress enhancement vs. MFR.

Table 3
Physical–mechanical features of base polymers (PP homopolymers + PP-*g*-MAH) and composites

	Standard deviation	Homo 1		Homo 2		Homo 3	
		Base polymer	Composite	Base polymer	Composite	Base polymer	Composite
Chord mod. (MPa)	10	1497	1909	1512	2112	1375	2051
Stress at 3.5% (MPa)	0.1	33.3	36.9	33.9	40.5	31.6	39.4
Yield strength (MPa)	0.1	34.5	36.5	34.4	36.7	32.7	35.1
Elong. at yield (%)	0.1	10.0	8.7	9.7	7.7	10.1	7.7
Elong. at break (%)	10	150	8	170	90	150	50
Impact str.-Izod (at 23 °C) (kJ/m^2)	0.1	3.5	3.0	3.7	3.7	2.6	2.6
HDT at 1.8 Mpa (°C)	2	55	58	54	58	52	59
4″ Length shr.[a] (in/in) 10^2	0.05	1.7	1.7	1.3	1.0	1.4	1.0
6″ Width shr.[b] (in/in) 10^2	0.05	1.9	1.7	1.3	1.0	1.4	1.0
CLTE 0–30 °C (10^{-5} °C^{-1})[c]	0.1	9.9	7.7	10.1	7.0	9.2	6.8
CLTE 30–60 °C (10^{-5} °C^{-1})[c]	0.1	12.0	10.5	12.5	9.5	11.4	9.0
CLTE 60–90 °C (10^{-5} °C^{-1})[c]	0.1	15.3	13.4	15.9	13.1	14.9	12.4
MFR (g/10 min)	0.1, 1, 2 Homo 1-2-3	0.5	0.4	6	4	25	18

[a] Length shr. = length shrinkage.
[b] Width shr. = width shrinkage.
[c] CLTE = coefficient of linear thermal expansion.

associated to the nanodispersion of the Cloisite 20A: indeed the value of Hetero 2 which is a microcomposite is the only one that is unaffected by addition of the organoclay (MFR: 1.5 and 1.6, respectively).

Impact strength was not affected by the clay in homopolymers whereas it tends to increase in heterophasic materials apart in the case of Hetero 3 in which a strong decrease was observed. Elongation at break strongly decreases only in the case of Homo 1, whilst it is much less affected in Homo 2 and Homo 3 and unaffected in the case of Hetero 1 and Hetero 2 showing even a strong increase in Hetero 3.

These data show that in rigid materials the nanofiller tends to act as a stress concentrator, constituting weak points that oppose plastic deformation, as in usual composites, whereas in rubbery phases the nanodispersed clays can follow the deformation of the macromolecules to which they are molecularly associated [20].

3.3. Thermal degradation

PP on heating at 10 °C/min thermally degrades to volatile products above 350 °C (Fig. 7) through a radical chain process propagated by carbon centred radicals (I and II, Scheme 1 [11]) originated by carbon–carbon bond scission [21]. Its weight loss begins at a much lower temperature in air than in nitrogen (above 200 °C, Fig. 7) and is completed before the temperature is reached for the process of Scheme 1 to take place. Indeed it is well known [21] that in presence of oxygen, PP undergoes the radical peroxidation chain process of Scheme 2 [11] starting at relatively low temperature (e.g. > 50 °C). With increasing the temperature, the carbon in chain radical that propagates peroxidation (III, Scheme 2) can undergo beta scission as shown by reaction 1 in Scheme 2. The resulting chain end radical (I) propagates volatilization of PP as in Scheme 1 with the additional possibility of partial further oxidation.

On increasing the temperature, also the allylic bond of fragments IV (indicated in Scheme 2) which are much weaker than original PP C–C bonds, can undergo thermal scission, further initiating the thermal volatilization of PP as in Scheme 1 by radicals I.

Above about 250 °C, peroxidation is overwhelmed by the radical chain oxidative dehydrogenation process of Scheme 2 [22]. Now, in chain C–C double bonds are created which, by thermal scission of the corresponding allylic C–C bond, provide radicals type V and II through reaction 2a that propagate PP volatilization as in Scheme 1. Also in this case the reaction of oxygen with the radicals can lead to partially oxidised volatiles.

Reaction 2 of Scheme 2 competes with volatilization of PP because further dehydrogenation of unsatured structures takes preferably place on allylic hydrogen leading to conjugated polyenes which are well known to be precursors of charred structures by rearrangement to aromatics or polyaromatics and crosslinking.

On programmed heating, in the presence of air, competition between reactions of Scheme 2 is largely in favour of volatilization as shown by the negligible residue left in Fig. 7 at the end of weight loss. In other words, oxygen catalyses the thermal degradation of PP increasing the rate of initiation that is of radicals formation.

Fig. 8 shows that the thermal degradation of the homopolymer nanocomposite in nitrogen is slightly delayed

Table 4
Physical–mechanical features of base polymers (heterophasic PP–PE + PP-*g*-MAH) and composites

	Standard deviation	Hetero 1		Hetero 2		Hetero 3	
		Base polymer	Composite	Base polymer	Composite	Base polymer	Composite
Chord mod. (MPa)	10	1345	1666	1409	1746	1308	1745
Stress at 3.5% (MPa)	0.1	29.2	30.3	29.9	30.9	29.1	32.2
Yield strength (Mpa)	0.1	28.6	29.2	28	27.9	26.4	27.9
Elong. at yield (%)	0.1	7.7	9.6	7.7	8.9	5.6	8.9
Elong. at break (%)	10	400	360	400	380	200	380
Impact str.-izod (at 23 °C) (kJ/m^2)	0.1	72.5	75.8	47.7	50.3	8.2	5.0
HDT at 1.8 Mpa (°C)	2	53	53	53	55	53	54
4″ Length shr.[a] (in/in) 10^2	0.05	1.6	1.6	1.1	1.1	1.4	1.4
6″ Width shr.[b] (in/in) 10^2	0.05	1.8	1.7	1.2	1.1	1.4	1.1
CLTE 0–30 °C (10^{-5} °C^{-1})[c]	0.1	8.9	7.5	7.6	6.8	11.6	8.1
CLTE 30−60 °C (10^{-5} °C^{-1})[c]	0.1	11.5	9.0	8.5	8.3	13.6	10.5
CLTE 60–90°C (10^{-5} °C^{-1})[c]	0.1	14.2	11.2	10.4	10.1	15.6	13.2
MFR (g/10 min)	0.1, 0.1, 1 Hetero 1-2-3	0.4	0.3	1.5	1.6	12	9.2

[a] Length shr. = length shrinkage.
[b] Width shr. = width shrinkage.
[c] CLTE = coefficient of linear thermal expansion.

in the early stage of weight loss ($T_{10\%}$, Table 5), whereas it is slightly accelerated during the main volatilization step (T_{peak}, Table 5).

The degradation of the homopolymer nanocomposite in air begins at about 220 °C as in the case of the pure homopolymer but, as the weight loss progresses, the material becomes apparently more stable than the matrix as it is shown by temperature of 10% weight loss (312 vs. 271 °C, Table 5) and temperature maximum rate of weight loss (431 vs. 314 °C, Table 5). Indeed about 40% of the composite volatilises above 400 °C that is the temperature range at which C–C bond of the PP chain undergo thermal scission. Thus, access of oxygen to the polymer matrix is progressively limited as the decomposition of the nanocomposite proceeds. The competition between charring and volatilization is not affected by the presence of the nanofiller since a negligible residue is obtained at the end of the volatilization process of the nanocomposites (Fig. 8) as in the case of the pure matrix (Fig. 7). On the other hand it was previously shown [9] that charring catalysis by the clay is detectable when heating is carried out in isothermal conditions at a relatively low temperature (230 °C). In

Table 5
TGA of base polymers (PP homopolymers + PP-*g*-MAH) and composites

	Standard deviation	Homo 1		Homo 2		Homo 3	
		Base polymer	Composite	Base polymer	Composite	Base polymer	Composite
$T_{10\%}$ (°C) in air	3	283	312	271	312	267	323
$T_{10\%}$ (°C) in nitrogen	2	426	433	425	433	421	423
T_{peak} (°C) in air	4	332	429	314	431	309	422
T_{peak} (°C) in nitrogen	4	455	446	458	447	455	448
Residue in air at 450 °C (%)	0.1	1.5	4.4	1.0	3.9	1.4	5.2

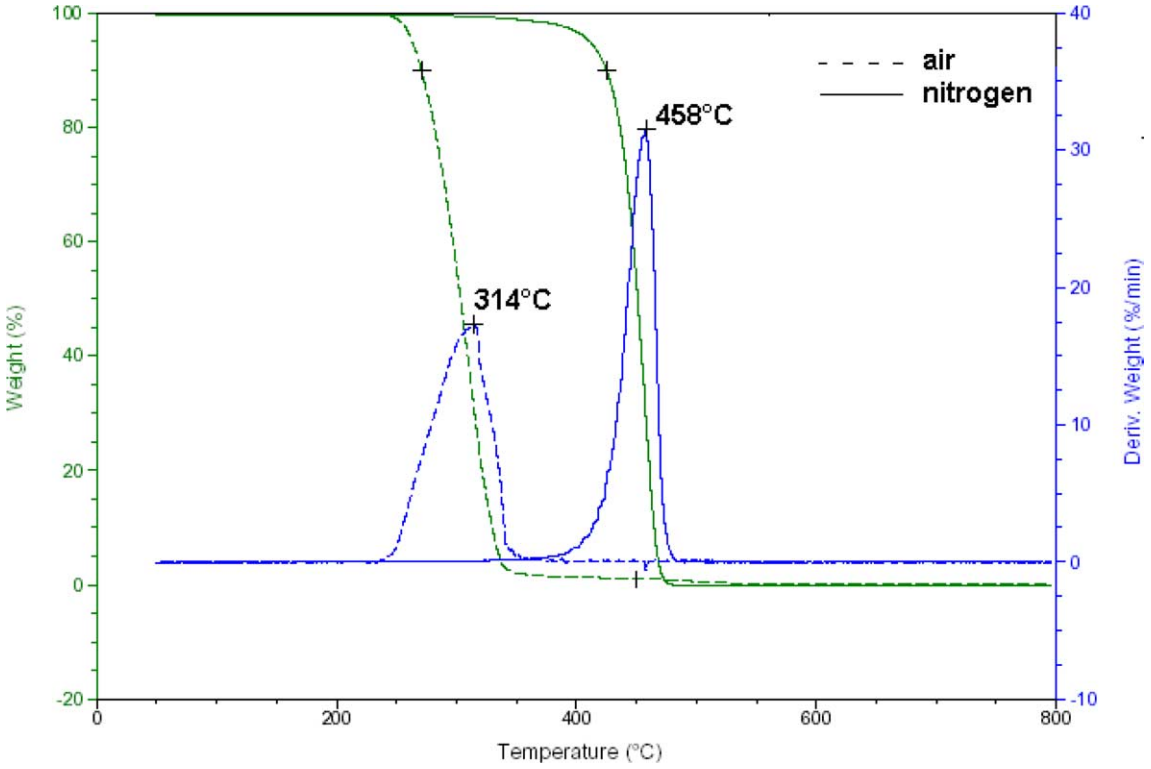

Fig. 7. TGA (air and nitrogen) of pure Homo 2.

these conditions volatilization is reduced and oxygen has time to diffuse and react with the polymer matrix and nanodispersed clay layers activated by the strong protonic acidic site left behind by thermal decomposition of the alkylammonium organic modifier ion [11].

The heterophasic copolymer nanocomposites show the same behaviour of the homopolymer nanocomposites in fact their thermal degradation is slightly delayed in the early stage of weight loss ($T_{10\%}$, Table 6), whereas it is slightly accelerated during the main volatilization step (T_{peak}, Table 6). In air the materials are more stable than the matrices as it is shown by temperature of 10% weight loss and temperature maximum rate of weight loss (Table 6).

4. Conclusions

The delamination of organoclays by melt blending is favoured at high MFR for both homopolymers and heterophasic copolymers. This is in contrast with literature data on polyamide 6 where a better delamination was obtained by increasing the molecular weight of the polymer [23]. The authors have attributed this result to the mechanical assistance to delamination of the clay by the larger shear stress in the extrusion process due to the larger melt viscosity of the polymer with larger molecular weight. In our case it seems that the organophilic environment, created in the layers interspace by combination of the organic cation and maleic anhydride grafted polypropylene, drives the delamination process through thermal diffusion control, making mechanical contribution negligible.

The expected increase in elastic modulus, typical of polymer–clay nanocomposites, is shown to be larger when delamination improves that is with increasing of melt flow rate of the polymer matrix. Increase of rigidity does not affect impact properties even for a 50% modulus increase (Homo 3, Table 3) which is also a behaviour typical of nanocomposites. Elongation at break is strongly reduced in homopolymers as

Scheme 1. Thermal degradation of PP.

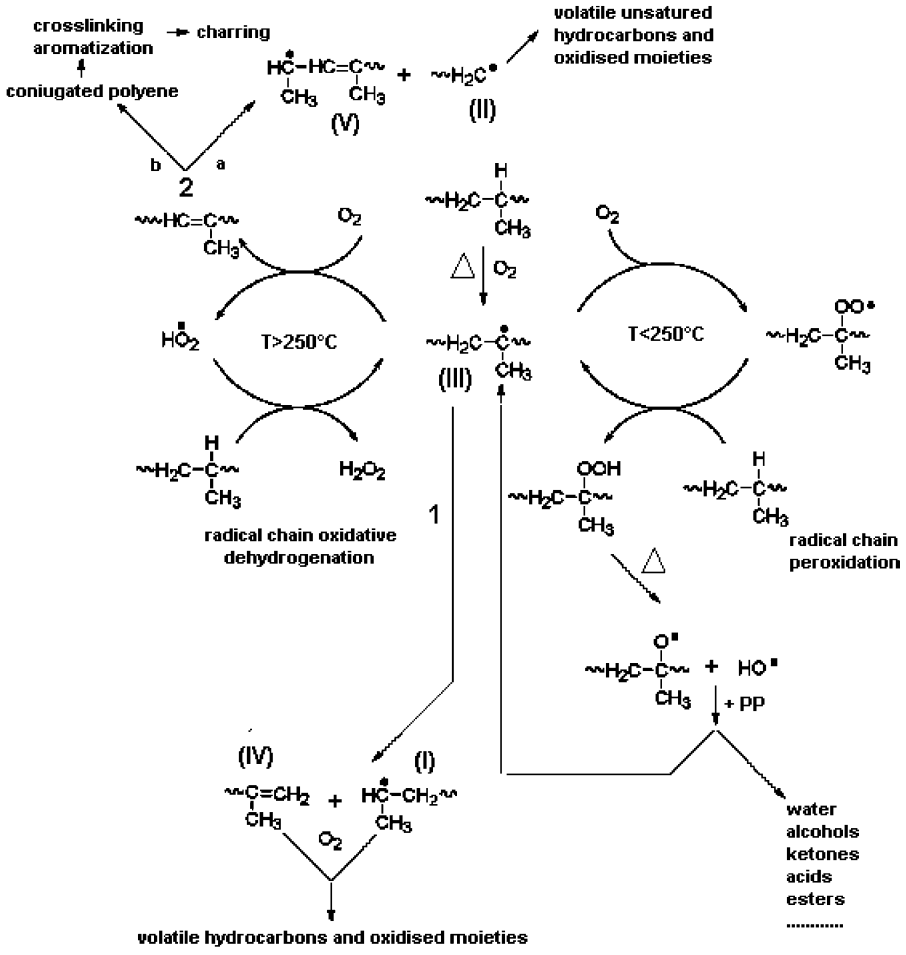

Scheme 2. Thermal oxidation of PP.

expected in composites, whereas it is unaffected in heterophasic materials or even increased when delamination is improved (Hetero 3, Table 4). A lower detrimental effect is also observed when delamination increases in homopolymers. This behaviour is to be attributed to the peculiar reinforcing mechanism of flexible clay layers intimately adhereing to the polymer chains which increase elastic modulus by hindering chain segmental rotation, but can follow chain unfolding when the mechanical stress overcomes bonds rotation constraint [20].

The presence of organoclay modifies the thermal oxidative volatilization behaviour of the polymer in all the composites, increasing the temperature at which volatilisation occurs. This should be due to a barrier labyrinth effect slowing down the diffusion rate of degradation products from the bulk of the polymer to the gas phase and also of oxygen from the gas phase into the polymer matrix. Volatilisation of the polymer leads to reassembling of the clay layers into the phyllosilicate structure, which creates a

Table 6
TGA of base polymers (heterophasic PP–PE + PP-*g*-MAH) and composites

	Standard deviation	Hetero 1		Hetero 2		Hetero 3	
		Base polymer	Composite	Base polymer	Composite	Base polymer	Composite
$T_{10\%}$ (°C) in air	3	282	331	271	320	206	306
$T_{10\%}$ (°C) in nitrogen	2	423	430	421	434	415	432
T_{peak} (°C) in air	4	314	443	301	428	276	413
T_{peak} (°C) in nitrogen	4	452	446	454	448	453	446
Residue in air at 450 °C (%)	0.1	1.5	6.2	1.4	5.6	1.2	4.8

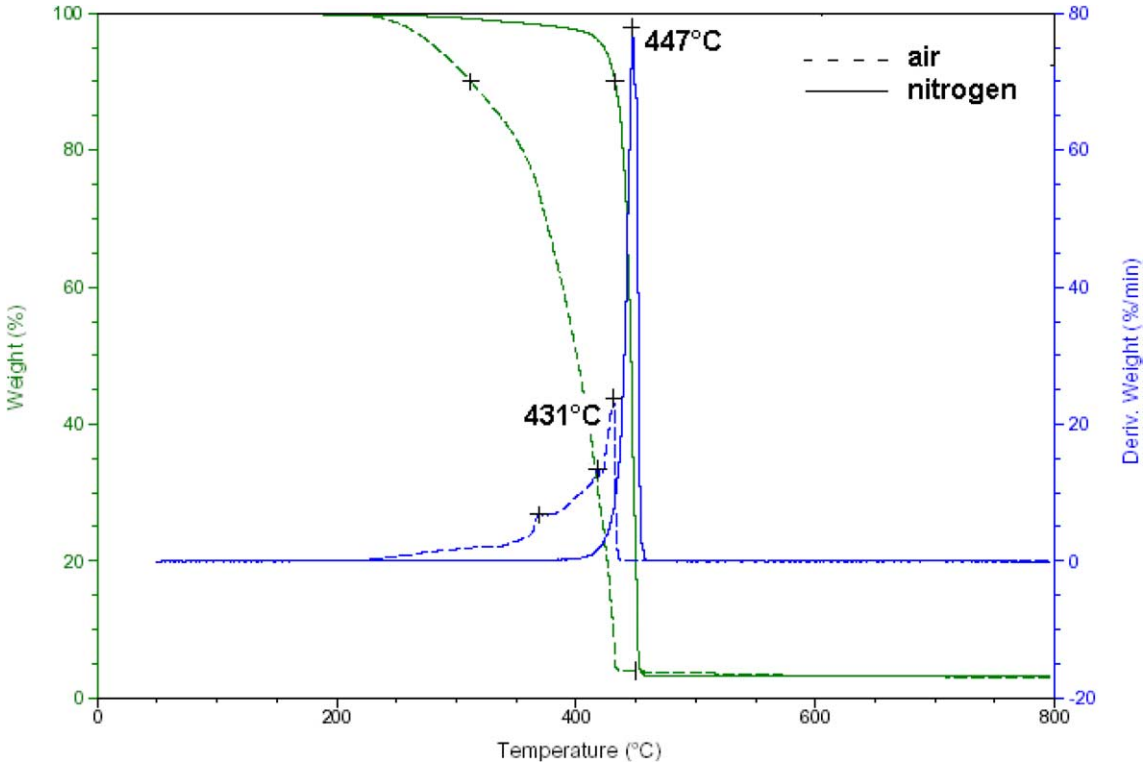

Fig. 8. TGA (air and nitrogen) of nanocomposite based on Homo 2.

surface ceramised skin that maximizes the protective barrier effect towards the underlying material. The fact that a similar behaviour is found for all the nanocomposites independently of their morphology indicates that effectiveness of the ablative reassembling process in providing the high temperature protective ceramised surface is apparently not affected by the type of clay delaminated morphology whether exfoliated or intercalated when heating occurs in dynamic conditions.

Acknowledgements

The Italian 'Ministero dell'Istruzione, dell'Università e della Ricerca' (MIUR, 'Fondo per gli Investimenti della Ricerca di Base', finanziamento 2001, Progetto MAPIO-NANO) is acknowledged for the financial support. The authors wish to thank M. Luciani and G. Ponzielli for their support in composites preparation, E. Arrobbio for thermogravimetric analyses and F. Fantinel for TEM measurements.

References

[1] Cox HL. Br J Appl Phys 1952;3:72–9.
[2] Hull D. An introduction to composite materials. London: Cambridge University Press; 1981.
[3] Zanetti M, Lomakin S, Camino G. Macromol Mater Eng 2000;279:1–9.
[4] Vaia RA, Jandt KD, Kramer EJ, Giannelis EP. Macromolecules 1995;28:8080–5.
[5] Liu LM, Qi ZN, Zhu YG. J Appl Polym Sci 1999;71:1133–8.
[6] Kawasumi M, Hasegawa N, Kato M, Usuki A, Okada A. Macromolecules 1997;30:6333–8.
[7] Oya A, Kurokawa Y, Yasuda H. J Mater Sci 2000;35:1045–50.
[8] Dennis HR, Hunter DL, Chang D, Kim S, White JL, Cho JW, et al. Polymer 2001;42:9513–22.
[9] Leuteritz A, Pospiech D, Kretzschmar B, Willeke M, Jehnichen D, Jentzsch U, et al. Adv Eng Mater 2003;9:678–81.
[10] Kaempfer D, Thomann R, Mülhaupt R. Polymer 2002;43:2909–16.
[11] Zanetti M, Camino G, Reichert P, Mülhaupt R. Macromol Rapid Commun 2001;22:176–80.
[12] Xu W, Liang G, Zhai H, Tang S, Hang G, Pan WP. Eur Polym J 2003;39:1467–74.
[13] Kretzschmar B, Pospiech D, Leuteritz A, Jehnichen D, Janke A, Tändler B. Process design for melt compounding of PP/clay-nanocomposites. Nanocomposites, San Francisco, USA 2003.
[14] Leuteritz A, Pospiech D, Kretzschmar B, Jehnichen D, Heger K, Jentzsch U, et al. Polym Mater Sci Eng 2002;87:297–9.
[15] Gianelli W, Camino G, Tzankova Dintcheva N, Lo Verso S, La Mantia FP. Macromol Mater Eng 2004;289:238–44.
[16] Kato M, Usuki A, Okada A. J Appl Polym Sci 1997;66:1781–5.
[17] Hasegawa N, Kawasumi M, Kato M, Usuki A, Okada A. J Appl Polym Sci 1998;67:87–92.
[18] Morgan AB, Gilman JW. J Appl Polym Sci 2002;87:1329–38.
[19] Hambir S, Bulakh N, Jog JP. Polym Eng Sci 2002;42:1800–7.
[20] Shah D, Maiti P, Jiang DD, Batt CA, Giannelis EP. Adv Mater 2005;17:525–8.
[21] Grassie N, Scott G. Polymer degradation and stabilization. Cambridge: Cambridge University Press; 1985.
[22] Benson SW, Nangia PS. Acc Chem Res 1979;12:223–8.
[23] Fornes TD, Yoon PJ, Keskkula H, Paul DR. Polymer 2001;42:9929–40.